Ultrafast Science
A SCIENCE PARTNER JOURNAL

RESEARCH ARTICLE

Probing Coupled Rotational and Electronic Dynamics during Laser-Induced Molecular Fragmentation

Keyu Guo[1†], Xiaoqing Hu[2†], Min Li[1*], Cong-Cong Jia[2], Songbin Zhang[3], Chuanpeng Cao[1], Wenhai Xie[1], Wei Cao[1], Kunlong Liu[1], Yueming Zhou[1], Yong Wu[2*], Jianguo Wang[2], and Peixiang Lu[1*]

[1]School of Physics and Wuhan National Laboratory for Optoelectronics, Huazhong University of Science and Technology, Wuhan 430074, China. [2]Key Laboratory of Computational Physics, Institute of Applied Physics and Computational Mathematics, Beijing 100088, China. [3]School of Physics and Information Technology, Shaanxi Normal University, Xi'an 710119, China.

*Address correspondence to: mli@hust.edu.cn (M.L.); wu_yong@iapcm.ac.cn (Y.W.); lupeixiang@hust.edu.cn (P.L.)
†These authors contributed equally to this work.

Citation: Guo K, Hu X, Li M, Jia CC, Zhang S, Cao C, Xie W, Cao W, Liu K, Zhou Y, et al. Probing Coupled Rotational and Electronic Dynamics during Laser-Induced Molecular Fragmentation. *Ultrafast Sci.* 2024;4:Article 0073. https://doi.org/10.34133/ultrafastscience.0073

Submitted 27 March 2024
Accepted 26 July 2024
Published 26 August 2024

Coupled nuclear and electronic dynamics within a molecule are key to understanding a broad range of fundamental physical and chemical processes. Although probing the coupled vibrational and electronic dynamics was demonstrated, it has so far been challenging to observe the coupling interactions between the rotational and electronic degrees of freedom. Here, we report the first observation of Coriolis coupling, a coupling interaction between nuclear rotational angular momentum and electronic axial angular momentum, during laser-induced molecular fragmentation by tracing the electronic structure of a dissociating O_2^+ molecule. We observe that the electron density changes its shape from that of a molecular σ orbital to a nearly isotropic shape as the internuclear distance goes up to ~20 Å, which results from the transition between nearly degenerate electronic states associated with different rotational angular momenta. Our experiment demonstrates that the breaking of a chemical bond does not occur suddenly during molecular dissociation. Instead, it lasts for a long time of several hundred femtoseconds due to the Coriolis coupling interaction. Our experiment can be extended to complicated molecules, holding the potential of revealing yet unobserved electron–nuclear coupling interactions during ultrafast processes.

Introduction

Probing and tracing electronic and nuclear dynamics in molecules on an ultrafast time scale is one of the ultimate goals of science, which is relevant to our understanding of many fundamental processes in physics and chemistry. With the development of ultrashort laser pulse, numerous methods have been demonstrated to probe and trace the rotational, vibrational, and electronic dynamics of molecules on picosecond, femtosecond, or even attosecond time scales, such as high-harmonic spectroscopy [1–3], ultrafast electron or x-ray diffraction [4–6], strong-field photoelectron holography [7–9], and time-resolved photoelectron spectroscopy [10–15]. Owing to the large mass difference between the nuclei and electrons, the nuclear motion is usually slower than the electron motion. Thus, in most cases, the molecular dynamics were understood within the Born–Oppenheimer approximation, in which the electronic and nuclear degrees of freedom are treated separately.

When a molecule is promoted to an electronically excited state in which the individual atoms are no longer in their equilibrium positions, the atoms may evolve to form a new molecular structure in which 2 electronic states become degenerate, e.g., at a conical intersection [16,17] or at a large internuclear distance. As a result, the electronic and nuclear dynamics occur on comparable time scales, and the electronic motion will be strongly coupled with the nuclear motion. The coupled motions of electrons and nuclei are ubiquitous in nearly all photochemical reactions [2,10,18–22], which determine the dominant pathways of charge or energy transfer for the reactions. Those coupled dynamics have been extensively studied in many ultrafast processes, such as molecular autoionization [11,23], interatomic Coulombic decay [24–27], and light-induced conical intersections [28–30]. However, all those previous studies focused on the coupling of electronic and vibrational degrees of freedom. Compared to vibrational motion, rotational motion occurs on a slower time scale, which is typically 5 or 6 orders of magnitude larger than the natural time scale of electron motion. Thus, the rotational dynamics can hardly be intertwined with the electronic dynamics [31]. Up to now, observing the direct interactions between the electronic and rotational degrees of freedom has remained unreached.

In this work, we report on a joint experimental and theoretical study of the coupled dynamics between the electronic and rotational degrees of freedom during ultrafast molecular dissociation. Using a time-resolved Coulomb explosion imaging method with circularly polarized pump and linearly polarized probe laser pulses, we trace the evolution of the transient electronic structure of O_2^+ for the internuclear distance from ~5 a.u. to ~40 a.u.[atomic units (a.u.) are used unless specified otherwise]. For such large internuclear distances, we find that Coriolis coupling, i.e., the coupling of molecular rotational angular momentum and electronic axial angular momentum, plays a dominant role, leading to a transition from the $1^4\Sigma_u^+$ electronic state to the neighboring $a^4\Pi_u$ electronic state of the O_2^+ molecule. This Coriolis coupling interaction was usually ignored in previous studies. Since both $1^4\Sigma_u^+$ and $a^4\Pi_u$ states dissociate into $O(^3P)$ and $O^+(^4S^0)$, their potential energy remains degenerate at relatively large internuclear distances. The Coriolis coupling process lasts for a long time of several hundred femtoseconds until the populations on the $1^4\Sigma_u^+$ and $a^4\Pi_u$ states become the same.

Methods

Experimental methods

Our measurements were performed in a reaction microscope of cold-target recoil-ion momentum spectroscopy (COLTRIMS) [32,33]. A linearly polarized femtosecond laser pulse (25 fs, 800 nm, 5 kHz) from a Ti:sapphire laser system was split in a Mach–Zehnder-type interferometer to produce a pump pulse and a probe pulse with a variable time delay. The pump pulse was changed to circular polarization using a quarter-wave plate. The resulting 2 pulses were afterward focused into a supersonic beam of O_2 molecules in the main chamber of the COLTRIMS, where the time of flight and the position of each ion were recorded. The temperature of the supersonic molecular beam was estimated to be almost 25 K. The intensities of the pump and probe pulses were estimated to be almost 3×10^{14} W/cm^2 and 1.5×10^{14} W/cm^2, respectively.

Our experimental scheme is shown in Fig. 1A. A circularly polarized femtosecond pump laser pulse is used to tunnel ionize an O_2 molecule. The potential energy curves shown in Fig. 1B are calculated using the complete active space self-consistent field (CASSCF) and multi-reference doubly excited configuration interaction (MRDCI) method, in which the orbital wave functions are expanded on Dunning's cc-pV5Z basis set [34]. In the CASSCF calculations, all the states formed by the coupling of the 2s and 2p electrons from 2 O atoms are optimized simultaneously. Then, the higher-precision MRDCI calculations are used to consider the configuration interactions. The active space is composed of all valence orbitals, with totally about 60,404, 71,464, and 148,290 contracted configurations and 2,124,204, 2,563,160, and 2,626,806 uncontracted configurations included in the configuration interaction calculations for O_2, O_2^+, and O_2^{2+}, respectively.

The singly ionized O_2^+ molecule will dissociate mainly along the $1^4\Sigma_u^+$ state as known from previous studies [35–37], as shown in Fig. 1B. After a variable time delay, the dissociating O_2^+ molecule is further ionized by a linearly polarized probe laser pulse, leading to Coulomb explosion of the molecule. The angular distribution of the resulting fragments is determined by the angular dependence of 2 ionization steps, i.e., the removal of the 2 electrons from the O_2 molecule [38–40]. Because the pump laser pulse is circularly polarized and the molecular axis is randomly aligned, the pump laser pulse contributes to an

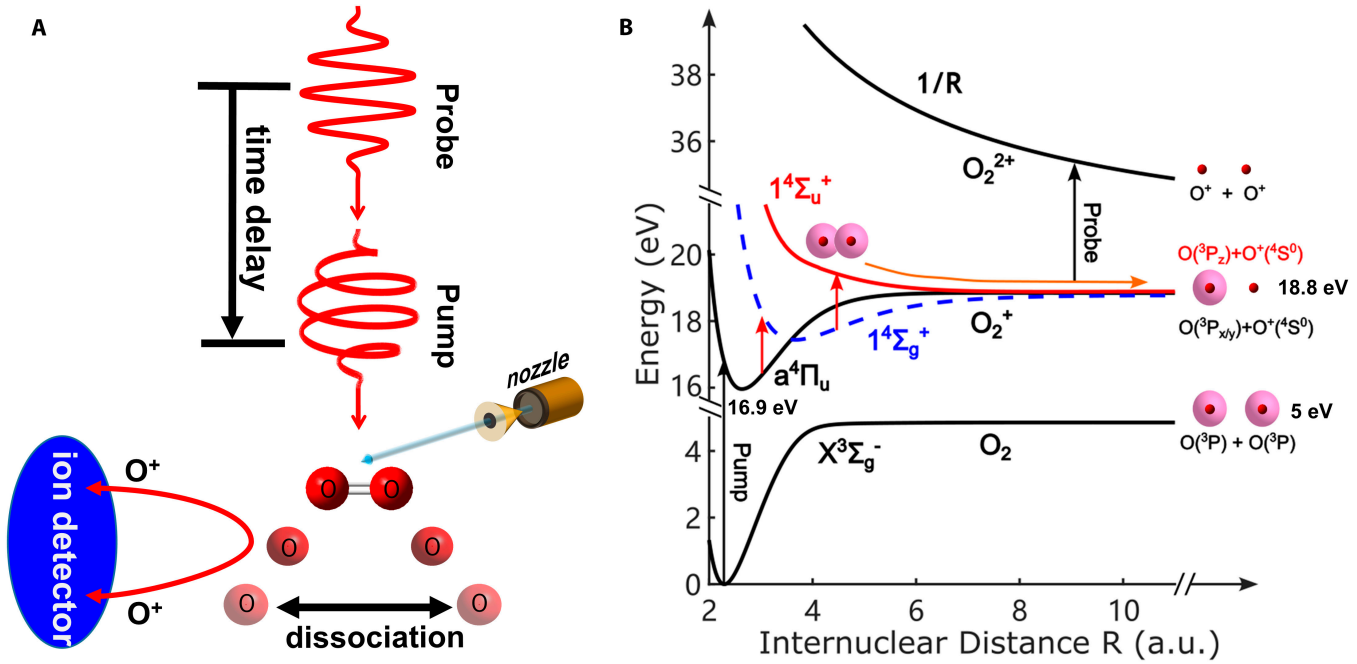

Fig. 1. (A) Schematic of tracing the evolution of the electronic structure in a dissociating molecule. An O_2 molecule is singly ionized by a circularly polarized pump laser pulse, initiating dissociation of O_2^+ molecule. After a variable time delay, the dissociating O_2^+ molecule is further ionized by a linearly polarized probe laser pulse, leading to Coulomb explosion. The time-dependent electronic structure of the dissociating molecule is mapped onto the angular distribution of the 2 resulting O^+ fragments. (B) Illustration of the dissociation of the O_2^+ molecule (see text for details). The dissociation limits are indicated at the right of the potential curves. Here, red vertical arrows represent 2 single-photon transitions following the tunneling ionization.

isotropic ionic angular distribution. Thus, the anisotropy of the angular distribution of the fragments will be determined by the removal of the second electron in the probe laser pulse, which directly reflects the electronic structure of the dissociating O_2^+ molecule [40,41]. Furthermore, the second electron of the dissociating O_2^+ molecule is released by the probe pulse, and then the Coulomb explosion starts to occur. The kinetic energy release (KER) of the fragments records the internuclear distance at the moment of the Coulomb explosion, i.e., when the probe pulse arrives. Thus, by tuning the pump-probe time delay, we can trace the evolution of the electronic structure of the dissociating O_2^+ molecule with the internuclear distance, from which the coupled nonadiabatic rovibronic dynamics can be revealed.

Quantum time-dependent wave packet simulations

In this work, a quantum time-dependent wave packet evolution method is used to simulate the breakup process [42], in which the whole nuclear dynamical processes from the neutral O_2 to the dissociated O_2^+ ion are considered.

First, we simulate the time-dependent evolution of the neutral O_2 molecular wave packets under the action of the strong laser field. Here, we mainly consider the excitation of the rotational states of the neutral O_2 molecule by the dipole polarization interaction between the laser and molecules. For this process, the Hamiltonian of the system is written as

$$\mathbf{H} = \left[\mathbf{H}_a(R,\ r_e) + \mathbf{R}\left(\overline{R}\right)\right] + \mathbf{R}(R) - \mathbf{R}\left(\overline{R}\right) + \mathbf{P} = \mathbf{H}_0 + \mathbf{H}'. \quad (1)$$

Here, $\mathbf{H}_a(R, r_e)$ is the adiabatic Hamiltonian that includes the electronic and nuclear kinetic energy, electron–electron, and electron–nuclear potential energy, where R and r_e are the internuclear distance and coordinates of the bound electrons, respectively. $\mathbf{R}$ is the rotational energy of O_2, which can be written as $\mathbf{R} = \frac{N(N+1)}{2\mu R^2}$, where μ is the molecular reduced mass, R is the internuclear distance, $\overline{R}$ is the equilibrium internuclear distance of the neutral O_2, and N is the rotational angular momentum. Considering that the O atom is boson, the spatial wave function of the O_2 molecule should be symmetric. Hence, the rotational quantum number N should be odd for the neutral O_2 ($X^3\Sigma_g^-$). Since $\overline{R}$ is set as a constant, the eigenstates of $\mathbf{H}_0$ can be written as $\psi_e^{q1}(R,\ r)\Psi(R)\Phi(\theta,\phi)$, where $\psi_e^{q1}(R,r)$ is the electronic wavefunction calculated by the ab initio method, $\Psi(R)$ is the molecular vibrational eigen wavefunction for *q1* electronic state obtained by solving the one-dimensional nuclear Schrödinger equation, and $\Phi(\theta,\phi)$ is the rotational wavefunction, which is expanded as the superposition of different spherical harmonic functions $Y_{Nm}(\theta,\phi)$. Here, the rotation and vibration are independent. $\mathbf{P}$ represents the polarization interaction between the laser and O_2 molecule and can be given as $-E(t)^2(\alpha_z\cos^2\gamma + \alpha_{x/y}\sin^2\gamma)$, where γ is the angle between the laser field relative to the direction of the O–O bond (z axis), and α_z and $\alpha_{x/y}$ are the axial and vertical dipole polarizability, respectively. The pump electric field $E(t)$ is circularly polarized and can be given as $E(t) = E_0 f(t)(\hat{\mathbf{e}}_x\sin(\omega t) + \hat{\mathbf{e}}_y\sin(\omega t + \pi/2))$, where $f(t) = \sin^2(\pi t/t_0)$ for $0 < t < t_0$ is the envelope function of the laser pulse. E_0, ω, and t_0 are the peak amplitude, the carrier frequency, and the pulse duration of the electric field, respectively.

Second, assuming that the first electron is released at the instant of T_1, we simulate the time-dependent evolution of the O_2^+ molecular wave packets under the action of the laser field. Here, the initial electronic state of O_2^+ is set as $a^4\Pi_u$, in which one electron from the HOMO-1 of O_2 (see below) is removed by the laser field. It is assumed that the strong-field ionization only changes the rotational wave packet of the molecule and does not change the vibrational state distribution. Because the ionization time T_1 determines the subsequent dynamical processes, we consider the impact of the ionization time of the neutral molecules O_2 on the fragmentation dynamics of O_2^+. For O_2^+, the Hamiltonian is written as

$$\mathbf{H} = \left[\mathbf{H}_a(R,\ r_e) + \mathbf{R}\left(\overline{R}\right)\right] + \mathbf{R}(R) - \mathbf{R}\left(\overline{R}\right) + \mathbf{E}\cdot\mathbf{D} + \mathcal{R} = \mathbf{H}_0 + \mathbf{H}', \quad (2)$$

where $\mathbf{E}\cdot\mathbf{D}$ represents the dipole interaction between the laser field and the O_2^+ ion. The Coriolis coupling interaction $\mathcal{R}$ is written as

$$\mathcal{R} = \frac{1}{\mu R^2}(\mathbf{J}_+ - \mathbf{J}_-)\left\langle \psi_e^{q1}\middle| i\mathbf{L}_y \middle|\psi_e^{q2}\right\rangle, \quad (3)$$

where $\mathbf{J}_+$ and $\mathbf{J}_-$ are the ascending and descending operators of the total angular momentum $\mathbf{J}$, $\mathbf{L}_y$ represents the angular momentum perpendicular to the molecular axis, and ψ_e^{q1} and ψ_e^{q2} are the electronic wave functions of the 2 electronic states *q1* and *q2*.

In our simulation, 4 electronic states of $a^4\Pi_{ux}$, $a^4\Pi_{uy}$, $1^4\Sigma_g^+$, and $1^4\Sigma_u^+$ for O_2^+ are considered simultaneously and 1,000 vibrational states for each electronic state are used to expand the wave packet $\Psi_{O_2^+}(r)$. The maximal rotational quantum number used is up to 30. We simulated the dipole transitions between $a^4\Pi_{ux/y}$ and $1^4\Sigma_g^+$, $1^4\Sigma_g^+$ and $1^4\Sigma_u^+$, and the Coriolis coupling between $a^4\Pi_{ux/y}$ and $1^4\Sigma_u^+$, $a^4\Pi_{ux}$ and $a^4\Pi_{uy}$, respectively. Then, we calculate a weight factor W_{N0m0T1} of each trajectory with different initial rotational angular momenta (N_0, m_0) and different ionization times T_1 (see the Supplementary Materials).

Based on the weight factor W_{N0m0T1}, the calculated Coriolis coupling matrix elements, and the simulated relative proportion of the p_x/p_y orbitals, we obtain the final relative proportion of the p_z orbital and p_x/p_y orbitals. Then, we use the partial Fourier transform method to obtain the angle-dependent ionization rate for the probing step at each internuclear distance [43,44], from which we calculate the value of $\langle\cos^2\theta\rangle$. Here, θ is the emission angle of O^+ relative to the polarization direction of the linearly polarized laser pulse [31], which allows us to separately study those effects on the ionic angular distribution.

Results

Figure 2A shows the measured KER distribution as a function of the pump-probe time delay for the Coulomb explosion channel of $O^+ + O^+$. The positive time delay means that the pump laser pulse is circularly polarized and the probe laser pulse is linearly polarized. The case is reversed for the negative time delay. One sees that there is a time-independent features at KER ~9 eV, which is mainly caused by the interaction with only the pump laser pulse. The KER spectrum also reveals a clear time-dependent feature, which reflects the behavior of parts of the

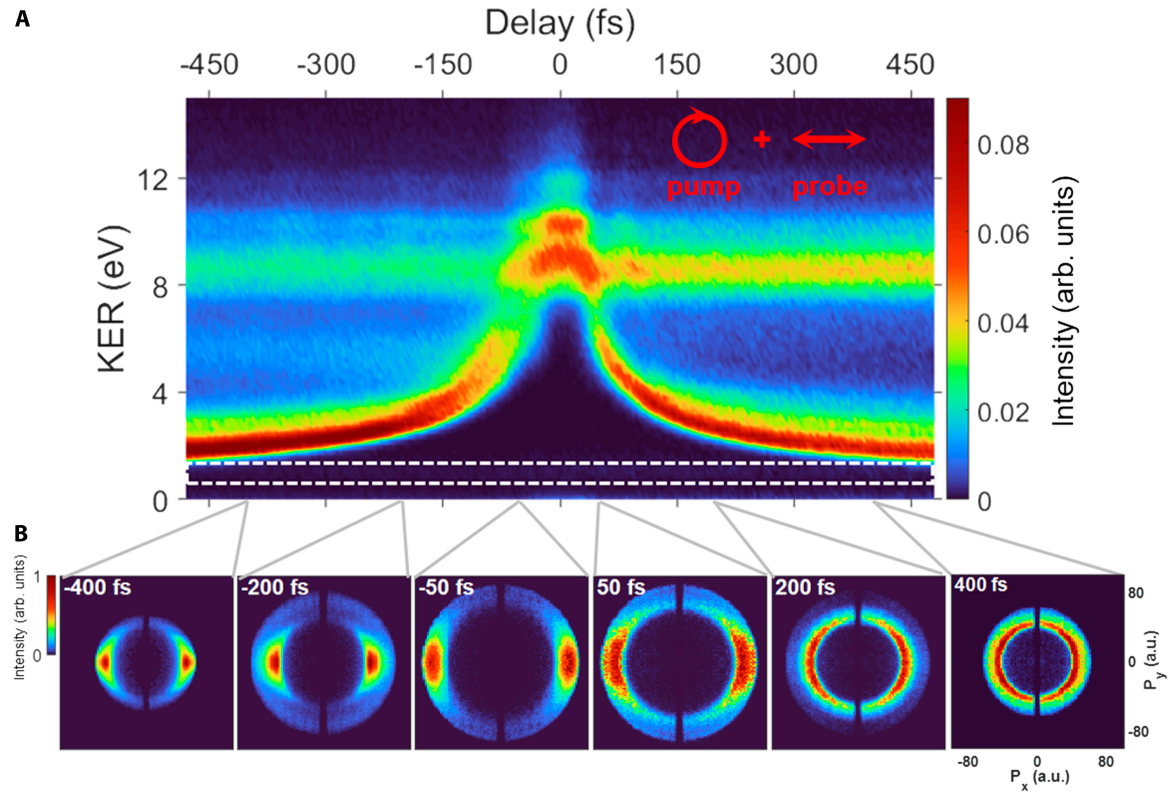

Fig. 2. (A) Measured ion yields from Coulomb explosion of O_2 molecule as a function of KER and the time delay between the pump and the probe pulses. The weak signal within the white dashed rectangle can be used to obtain the asymptotic KER. (B) Measured momentum distributions of 2 coincident O^+ fragments at several specific time delays for KER <7 eV. The polarization direction of the probe pulse is along the horizontal direction.

nuclear wave packet induced by both laser pulses. The KER of the time-dependent feature decreases gradually as a function of time from ~9 eV to the asymptotic energy of ~1.2 eV. The asymptotic KER of ~1.2 eV is obtained by the weak signal of the bond softening of O_2^+ [45], as shown by the white dashed rectangle in Fig. 2A.

The asymptotic KERs allow assigning the dissociation pathway involved. Because removal of an electron from the highest occupied molecular orbital (HOMO) corresponds to a nondissociative state of O_2^+, i.e., $X^2\Pi_g$, the dissociative ionization is dominated by the removal of an electron from the HOMO-1 of O_2 [46]. The ionization from HOMO-1 will result in a strong population on the $a^4\Pi_u$ state (~16.9 eV in the potential energy curve) by an adiabatic Franck–Condon type transition. Then, the O_2^+ on $a^4\Pi_u$ state can further be promoted into a dissociative $1^4\Sigma_u^+$ state with a dissociation limit at ~18.8 eV by 2 single-photon transitions [35–37], as indicated by the 2 vertical red arrows in Fig. 1B. The asymptotic energy release about 1.2 eV can be assigned to the dissociation pathway $\left|a^4\Pi_u\right\rangle \rightarrow \left|1^4\Sigma_g^+ - \omega\right\rangle \rightarrow \left|1^4\Sigma_u^+ - 2\omega\right\rangle$ as shown in Fig. 1B, where ω is the laser frequency.

Figure 2B shows the momentum distributions of the 2 coincident O^+ fragments for the time-dependent feature (KER <7 eV) at several specific time delays. For the positive time delay, the momentum distribution is mainly along the horizontal direction for the time delay of ~50 fs, while it changes to a nearly isotropic ring with increasing the time delay. In contrast, for the negative time delay, the ions are mainly emitted along the horizontal direction for all time delays.

The ionic angular distribution is determined by the angular dependence of 2 ionization steps [38–40]. For the negative time delay, the angular distribution of the fragments is mainly determined by the removal of the first electron in the linearly polarized laser field. Because the removal of the first electron is always from the equilibrium internuclear distance of the O_2 molecule, the angular distribution of the fragments is nearly unchanged with the time delay. For the positive delay, the angular distribution of the fragments is determined by the angular dependence of the removal of the second electron from the dissociating O_2^+ molecule in the linearly polarized probe pulse. For tunneling ionization of randomly aligned molecules by a linearly polarized laser pulse, the ionic angular distribution is equivalent to the angle-dependent ionization yield for a fixed molecular orientation, i.e., molecular frame ionization yield. It has been shown that the molecular frame ionization yield directly reflects the electron density distribution in the valence shells of a molecule [40,41]. Thus, the angular distribution of the coincident ion pairs maps the evolution of the electronic density distribution of the dissociating O_2^+ molecule.

To quantitatively show the evolution of the electronic structure with time, we use the expectation value of $\cos^2\theta$ to characterize the ionic angular distribution [47], which is written as $\left\langle \cos^2\theta \right\rangle = \frac{\int I(\theta)\cos^2\theta\sin(\theta)d\theta}{\int I(\theta)\sin(\theta)d\theta}$. Here, $I(\theta)$ is the ionic angular

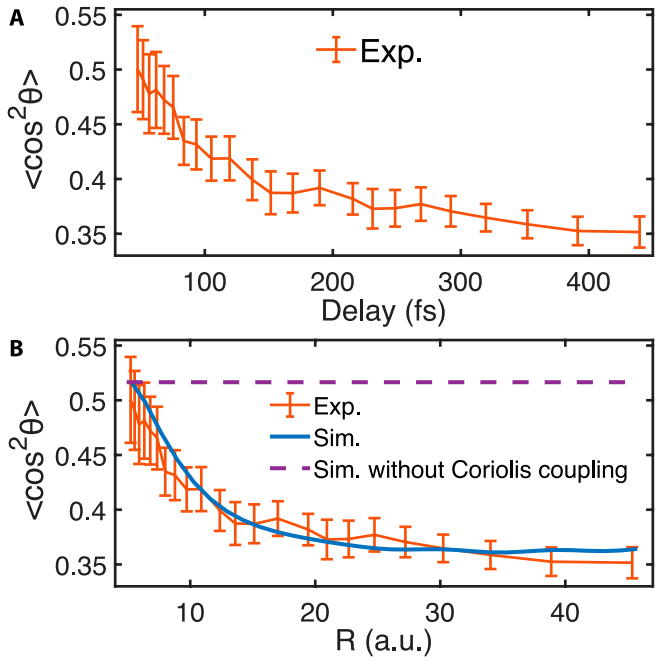

Fig. 3. (A) Measured $<\cos^2\theta>$ with respect to the time delay between the pump and probe laser pulses. (B) Measured and simulated $<\cos^2\theta>$ with respect to the internuclear distance R of the molecule.

distribution. $\langle\cos^2\theta\rangle = 1/3$ for an isotropic angular distribution. Figure 3A shows the measured $\langle\cos^2\theta\rangle$ as a function of the pump-probe time delay (for positive delays). One sees that $\langle\cos^2\theta\rangle$ decreases rapidly with the time delay within the first 50 to 100 fs and does not reach 1/3 after 400 fs. This means that the polarization of the electronic density distribution is lost during the dissociation process. For the Coulomb explosion of a diatomic molecule, KER is given by the instantaneous internuclear distance R of the molecule when the probe pulse arrives, which can be expressed as $KER(\tau) = 1/R(\tau) + E_0$ [45], where τ is the delay and E_0 is the kinetic energy of the corresponding dissociation process. E_0 is the asymptotic energy release, which equals ~1.2 eV according to Fig. 2A. The time-dependent feature in Fig. 2A reveals a direct correspondence between the delay and KER, making it possible to resolve the internuclear distance for different delays, that is, $R(\tau)$. Thus, as shown in Fig. 3B, we obtain the evolution of the electronic structure of the dissociating O_2^+ molecule for the internuclear distance from ~5 a.u. to ~40 a.u.

Discussion

We have performed quantum time-dependent wave packet simulations for the dissociation of O_2^+, which has included Coriolis coupling between nuclear rotational angular momentum and electronic axial angular momentum. We achieve a good agreement between the measurement and the simulation, as shown in Fig. 3B. It should be noted that the effects of ionization, coupling transition between different electronic states, and molecular reorientation on the ionic angular distributions have all been taken into account in the simulation. During the molecular fragmentation processes, there are several types of interactions that can cause the transition of electronic states and change the orbital shape, i.e., the spontaneous radiation, radial coupling interaction at a conical intersection, the spin-orbit coupling, and the Coriolis coupling. The lifetime of spontaneous radiation is generally in the nanosecond scale. Therefore, this process can be ignored in our study. For the radial coupling interaction, there is no conical intersection in our present research. For the spin-orbit coupling, the transition intensity will decrease rapidly with the increase of the internuclear distance. Therefore, the spin-orbit coupling can also be ignored. The Coriolis coupling interaction between the molecular rotational angular momentum and electron orbital angular momentum is the only one interaction that can cause continuous changes in molecular orbitals within a few hundred femtoseconds. Among the above interactions, our experimental results can only be explained by the Coriolis coupling. As shown by the dashed line in Fig. 3B, if we remove the Coriolis coupling interaction in the simulation, the shape of the electronic structure would not change with the internuclear distance.

Because the internuclear distance of the dissociating O_2^+ molecule is large in our experiment, the molecular orbital for the electron localized on the neutral O nuclei can be considered as a combination of atomic p orbitals (including p_x, p_y, and p_z). Here, z represents the molecular axis direction and x and y represent the 2 directions perpendicular to the molecular axis. To shed light on how the Coriolis coupling affects the molecular electronic structure, we show in Fig. 4A the calculated relative contribution of the atomic p_z orbital and the atomic p_x or p_y orbitals to the electronic structure as a function of the internuclear distance. We can see that the relative contribution of the p_x (or p_y) orbital increases while the relative contribution of the p_z orbital decreases with increasing the internuclear distance. For a dissociated O_2^+ ion with a large internuclear distance, the $1^4\Sigma_u^+$ state corresponds to the coupling of the atomic p_z orbital with the $O^+(\,^4S^0)$ and the $a^4\Pi_u$ state corresponds to the coupling of the atomic p_x or p_y orbitals with the $O^+(\,^4S^0)$. Therefore, the increase of the relative contribution of the p_x (or p_y) orbital means that there is a transition from the $1^4\Sigma_u^+$ state to the $a^4\Pi_u$ state during the dissociation process due to the Coriolis coupling. However, the populations on the $1^4\Sigma_u^+$ and $a^4\Pi_u$ states do not converge to 1/3 even at a large internuclear distance of R= 40 a.u. The main reason is that the Coriolis coupling strength depends on the nuclear rotational angular momentum N. Figure 4B shows the proportion of the p_x orbital to the electronic structure for different N ($N \geq 1$ and N is odd). As can be seen, the proportion of the p_x orbital approaches to 1/3 faster for larger N. This can be explained remarkably simply: A larger nuclear rotational angular momentum corresponds to a larger Coriolis force for the electron, leading to a larger Coriolis coupling strength. As a result, within the first 50 to 100 fs (the internuclear distance changes from 5.5 to 10 a.u.), all rotational angular momenta contribute to the electronic transition induced by the Coriolis coupling. Thus, the polarization of the electronic density distribution is mainly lost during this time interval, as shown in Fig. 3A. For a larger time delay, the electronic transition induced by the Coriolis coupling is only contributed by small N, which leads to a smaller transition rate. Since the Coriolis coupling strength is small for small N (e.g., $N = 1$), the electronic transition induced by the Coriolis coupling for small N is still not balanced after 400 fs (corresponding to the internuclear distance of ~40 a.u.). Thus, the Coriolis coupling process lasts several hundred femtoseconds

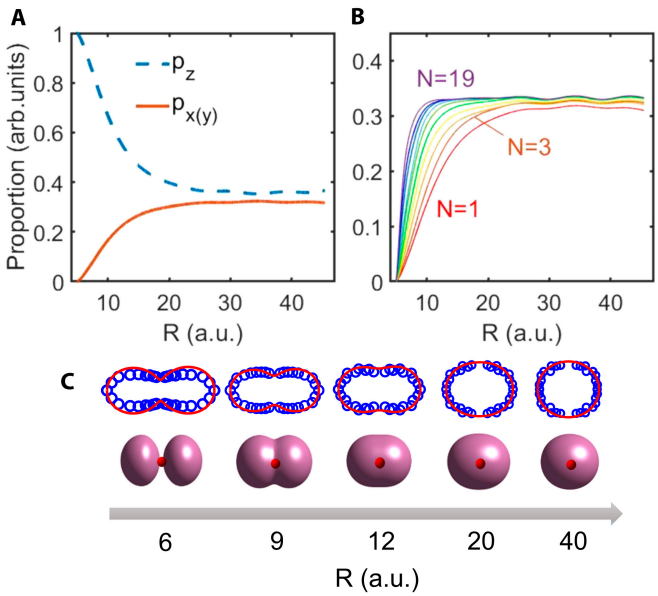

Fig. 4. (A) Calculated relative proportion of the p_z orbital (dashed line) and p_x/p_y orbitals (solid line) to the molecular electronic structure with respect to the internuclear distance. (B) Calculated relative proportion of the p_x/p_y orbitals with respect to the internuclear distance for initial nuclear rotational angular momentum N changing from N=1 to N=19. (C) The top row shows the measured and simulated angular distributions of O^+ for different internuclear distances. The blue circles and the red solid lines are the measured and simulated results, respectively. The bottom row shows the calculated spatial density distribution of the electron localized on the neutral O nuclei for the dissociating O_2^+ molecule. The red dots indicate the core of the neutral O atom, and the internuclear axis is along the horizontal direction.

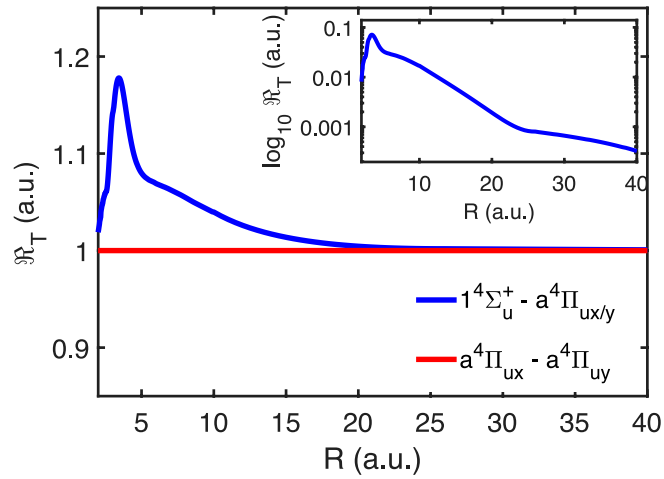

Fig. 5. The calculated Coriolis coupling matrix elements $\Re_T$ between the $1^4\Sigma_u^+$ and $a^4\Pi_{ux/y}$ states (blue line) and between the $a^4\Pi_{ux}$ and $a^4\Pi_{uy}$ states (red line) with respect to the internuclear distance. The inset shows $\log_{10}\Re_T$ on a logarithmic scale with respect to the internuclear distance, where the red line is located at zero.

until the proportions of the p_z and p_x (or p_y) orbitals become the same.

We show in Fig. 5 the calculated Coriolis coupling matrix elements between the $1^4\Sigma_u^+$ and $a^4\Pi_{ux/y}$ states (blue line) and between the $a^4\Pi_{ux}$ and $a^4\Pi_{uy}$ states (red line) with respect to the internuclear distance. One can see that the rotational coupling is strong at short internuclear distances. However, when the internuclear distance is as large as ~40 a.u., the coupling matrix element between the $1^4\Sigma_u^+$ and $a^4\Pi_{ux/y}$ states is not equal to the coupling matrix element between the $a^4\Pi_{ux}$ and $a^4\Pi_{uy}$ states, as shown in the inset of Fig. 5. As a result, the electronic transition induced by the Coriolis coupling is not balanced at such large internuclear distance. Due to the fact that Coriolis coupling is a weak interaction, its influence on the diabatic potential energy curve is also weak. According to our calculation, at an O–O bond length of 10 a.u., the energy shift from the adiabatic potential energy to the diabatic potential energy is only 4.4×10^{-6} a.u. This small energy shift means a slow transition rate, corresponding to a very long transition time. This is the reason why the Coriolis coupling interaction lasts several hundred femtoseconds.

Using the simulated proportions of p_z and p_x (or p_y) orbitals in Fig. 4A, we obtain the transient electron density distribution for each internuclear distance (see Section S2). As shown in Fig. 4C, the electron density changes its shape from that of a molecular σ orbital to a nearly isotropic shape as the internuclear distance increases, which is consistent with the measured ionic angular distributions. The observed shape change is associated with the splitting and degeneracy of the energy levels of the 3 orbitals (p_x, p_y, and p_z) of O (^{3}P) in the O_2^+ molecule, which is directly related to the breaking of the O–O bond. For an isolated O (^{3}P) atom, the energy levels of the 3 orbitals are degenerate. After coupling with a neighboring O^+ ($^4S^0$), an energy splitting appears between the $p_{x/y}$ ($a^4\Pi_u$) and p_z ($1^4\Sigma_u^+$) orbitals since the symmetry between the axial (z) and vertical (x/y) directions is broken. This energy splitting leads to the fact that the $a^4\Pi_u$ and $1^4\Sigma_u^+$ electronic states undergo completely different nuclear dynamics. As a result, the generated fragments are dominated by the contributions from O (^3P_z) at a relatively small internuclear distance. With the stretching of the O–O bond, the energy levels of the p_x (or p_y) and p_z orbitals become degenerate, and the populations on the p_x, p_y, and p_z orbitals gradually become the same under the effect of Coriolis coupling. For O_2^+, the Coriolis coupling occurs in the transition from the $1^4\Sigma_u^+$ state to the $a^4\Pi_u$ state, until the proportions of the p_z and p_x (or p_y) orbitals become the same. Thus, we can observe the Coriolis coupling effect from the measured ionic angular distribution in the O_2 molecules. This is the reason why we choose O_2 molecule as the target.

In conclusion, we have traced the time evolution of the electronic structure in a dissociating O_2^+ molecule. We observe that the electronic density changes its shape from that of a molecular σ orbital to a nearly isotropic shape as the internuclear distance increases during the molecular dissociation process. The shape change is observed, compared to theory, which yields agreement only if the nonadiabatic Coriolis interaction is included in the calculation, proving that the nonadiabatic Coriolis coupling plays an important role during the transition from a molecule to atoms. We show that the breaking of the chemical bond in O_2 molecules does not occur at a certain moment. Instead, it lasts for a long time of several hundred femtoseconds due to the Coriolis coupling interaction. Our result provides new physical insights into how the O_2 molecule evolves into 2 O fragments. This finding has a strong impact on the elucidation of elementary reaction mechanisms in some photochemical reactions.

Acknowledgments

Funding: This work was supported by the National Key Research and Development Program of China (grant no. 2023YFA1406800) and the National Natural Science Foundation of China (grant nos. 62275085, 12021004, 11934004, and 12104063).
Author contributions: K.G., M.L., C.C., W.X., W.C., K.L., Y.Z., and P.L. designed the experiment and carried out the measurement. X.H., C.-C.J., S.Z., Y.W., and J.W. performed the calculations. K.G., X.H., M.L., S.Z., Y.W., and P.L. prepared the manuscript. All authors contributed to finalizing and approving the manuscript.
Competing interests: The authors declare that they have no competing interests.

Data Availability

The data that support the findings of this study are available within the article.

Supplementary Materials

Figs. S1 to S8
Sections S1 and S2
References

References

1. Baker S, Robinson JS, Haworth CA, Teng H, Smith RA, Chirilă CC, Lein M, Tisch JWG, Marangos JP. Probing proton dynamics in molecules on an attosecond time scale. *Science*. 2006;312(5772):424–427.
2. Wörner HJ, Bertrand JB, Kartashov DV, Corkum PB, Villeneuve DM. Following a chemical reaction using high-harmonic interferometry. *Nature*. 2010;466(7306):604–607.
3. He L, Lan P, Le A-T, Wang B, Wang B, Zhu X, Lu P, Lin CD. Real-time observation of molecular spinning with angular high-harmonic spectroscopy. *Phys Rev Lett*. 2018;121: Article 163201.
4. Wolter B, Pullen MG, Le A-T, Baudisch M, Doblhoff-Dier K, Senftleben A, Hemmer M, Schröter CD, Ullrich J, Pfeifer T, et al. Ultrafast electron diffraction imaging of bond breaking in di-ionized acetylene. *Science*. 2016;354(6310):308–312.
5. Yang J, Zhu X, Wolf TJ, Li Z, Pedro Nunes JF, Coffee R, Cryan JP, Gühr M, Hegazy K, Heinz TF, et al. Imaging CF_3I conical intersection and photodissociation dynamics with ultrafast electron diffraction. *Science*. 2018;361(6397):64–67.
6. Minitti MP, Budarz JM, Kirrander A, Robinson JS, Ratner D, Lane TJ, Zhu D, Glownia JM, Kozina M, Lemke HT, et al. Imaging molecular motion: Femtosecond X-ray scattering of an electrocyclic chemical reaction. *Phys Rev Lett*. 2015;114:Article 255501.
7. Huismans Y, Rouzée A, Gijsbertsen A, Jungmann JH, Smolkowska AS, Logman PSWM, Lépine F, Cauchy C, Zamith S, Marchenko T, et al. Time-resolved holography with photoelectrons. *Science*. 2011;331(6013):61–64.
8. Li M, Xie H, Cao W, Luo S, Tan J, Feng Y, Du B, Zhang W, Li Y, Zhang Q, et al. Photoelectron holographic interferometry to probe the longitudinal momentum offset at the tunnel exit. *Phys Rev Lett*. 2019;122:Article 183202.
9. Xie W, Yan J, Li M, Cao C, Guo K, Zhou Y, Lu P. Picometer-resolved photoemission position within the molecule by strong-field photoelectron holography. *Phys Rev Lett*. 2021;127:Article 263202.
10. Geßner O, Lee AM, Shaffer JP, Reisler H, Levchenko SV, Krylov AI, Underwood JG, Shi H, East AL, Wardlaw DM, et al. Femtosecond multidimensional imaging of a molecular dissociation. *Science*. 2006;311(5758):219–222.
11. Sandhu AS, Gagnon E, Santra R, Sharma V, Li W, Ho P, Ranitovic P, Cocke CL, Murnane MM, Kapteyn HC. Observing the creation of electronic Feshbach resonances in soft X-ray-induced O_2 dissociation. *Science*. 2008;322(5904): 1081–1085.
12. Bisgaard CZ, Clarkin OJ, Wu G, Lee AMD, Geßner O, Hayden CC, Stolow A. Time-resolved molecular frame dynamics of fixed-in-space CS_2 molecules. *Science*. 2009;323(5920):1464–1468.
13. von Conta A, Tehlar A, Schletter A, Arasaki Y, Takatsuka K, Wörner HJ. Conical-intersection dynamics and ground-state chemistry probed by extreme-ultraviolet time-resolved photoelectron spectroscopy. *Nat Commun*. 2018;9:3162.
14. Yu M, Liu K, Li M, Yan J, Cao C, Tan J, Liang J, Guo K, Cao W, Lan P, et al. Full experimental determination of tunneling time with attosecond-scale streaking method. *Light Sci Appl*. 2022;11:215.
15. Pan S, Hu C, Zhang Z, Lu P, Lu C, Zhou L, Wang J, Sun F, Qiang J, Li H, et al. Low-energy protons in strong-field dissociation of H_2^+ via dipole-transitions at large bond lengths. *Ultrafast Sci*. 2022;2022:9863548.
16. Herzberg G, Longuet-Higgins HC. Intersection of potential energy surfaces in polyatomic molecules. *Discuss Faraday Soc*. 1963;35:77–82.
17. Jadoun D, Kowalewski M. Tracking conical intersections with nonlinear x-ray Raman spectroscopy. *Ultrafast Sci*. 2022;2022:0003.
18. Li W, Zhou X, Lock R, Patchkovskii S, Stolow A, Kapteyn HC, Murnane MM. Time-resolved dynamics in N_2O_4 probed using high harmonic generation. *Science*. 2008;322(5905):1207–1211.
19. Zhou X, Ranitovic P, Hogle CW, Eland JH, Kapteyn HC, Murnane MM. Probing and controlling non-Born-Oppenheimer dynamics in highly excited molecular ions. *Nat Phys*. 2012;8:232–237.
20. Kobayashi T, Saito T, Ohtani H. Real-time spectroscopy of transition states in bacteriorhodopsin during retinal isomerization. *Nature*. 2001;414:531–534.
21. Polli D, Altoè P, Weingart O, Spillane KM, Manzoni C, Brida D, Tomasello G, Orlandi G, Kukura P, Mathies RA, et al. Conical intersection dynamics of the primary photoisomerization event in vision. *Nature*. 2010;467: 440–443.
22. Pan S, Hu C, Zhang W, Zhang Z, Zhou L, Lu C, Lu P, Ni H, Wu J, He F. Rabi oscillations in a stretching molecule. *Light Sci Appl*. 2023;12:35.
23. Gagnon E, Ranitovic P, Tong X-M, Cocke CL, Murnane MM, Kapteyn HC, Sandhu AS. Soft x-ray-driven femtosecond molecular dynamics. *Science*. 2007;317(5843):1374–1378.
24. Santra R, Zobeley J, Cederbaum LS, Moiseyev N. Interatomic coulombic decay in van der Waals clusters and impact of nuclear motion. *Phys Rev Lett*. 2000;85:4490–4493.
25. Jahnke T, Czasch A, Schöffler MS, Schössler S, Knapp A, Käsz M, Titze J, Wimmer C, Kreidi K, Grisenti RE, et al.

Experimental observation of interatomic coulombic decay in neon dimers. *Phys Rev Lett*. 2004;93:Article 163401.
26. Kuleff AI, Cederbaum LS. Tracing ultrafast interatomic electronic decay processes in real time and space. *Phys Rev Lett*. 2007;98:Article 083201.
27. Sisourat N, Kryzhevoi NV, Kolorenc P, Scheit S, Jahnke T, Cederbaum LS. Ultralong-range energy transfer by interatomic coulombic decay in an extreme quantum system. *Nat Phys*. 2010;6:508–511.
28. Corrales ME, González-Vázquez J, Balerdi G, Solá IR, De Nalda R, Bañares L. Control of ultrafast molecular photodissociation by laser-field-induced potentials. *Nat Chem*. 2014;6(9):785–790.
29. Natan A, Ware MR, Prabhudesai VS, Lev U, Bruner BD, Heber O, Bucksbaum PH. Observation of quantum interferences via light-induced conical intersections in diatomic molecules. *Phys Rev Lett*. 2016;116:Article 143004.
30. Kübel M, Spanner M, Dube Z, Naumov AY, Chelkowski S, Bandrauk AD, Vrakking MJ, Corkum PB, Villeneuve DM, Staudte A. Probing multiphoton light-induced molecular potentials. *Nat Commun*. 2020;11:2596.
31. Zhang SB, Wu Y, Wang JG. Time-dependent quantum wave packet dynamics to study charge transfer in heavy particle collisions. *J Chem Phys*. 2016;145:Article 224306.
32. Dörner R, Mergel V, Jagutzki O, Spielberger L, Ullrich J, Moshammer R, Schmidt-Böcking H. Cold target recoil ion momentum spectroscopy: A 'momentum microscope' to view atomic collision dynamics. *Phys Rep*. 2000;330:95–192.
33. Ullrich J, Moshammer R, Dorn A, Dörner R, Schmidt LPH, Schmidt-Böcking H. Recoil-ion and electron momentum spectroscopy: Reaction-microscopes. *Rep Prog Phys*. 2003;66:1463.
34. Buenker RJ, Peyerimhoff SD. Individualized configuration selection in CI calculations with subsequent energy extrapolation. *Theor Chim Acta*. 1974;35:33–58.
35. De S, Magrakvelidze M, Bocharova IA, Ray D, Cao W, Znakovskaya I, Li H, Wang Z, Laurent G, Thumm U, et al. Following dynamic nuclear wave packets in N_2, O_2 and CO with few-cycle infrared pulses. *Phys Rev A*. 2011;84:Article 043410.
36. Sen A, Sairam T, Sahu SR, Bapat B, Gopal R, Sharma V. Hindered alignment in ultrashort, intense laser-induced fragmentation of O_2. *J Chem Phys*. 2020;152:014302.
37. Xue S, Du H, Hu B, Lin CD, Le AT. Following coherent multichannel nuclear wave packets in pump-probe studies of O_2 with ultrashort laser pulses. *Phys Rev A*. 2018;97:Article 043409.
38. Alnaser AS, Voss S, Tong XM, Maharjan CM, Ranitovic P, Ulrich B, Osipov T, Shan B, Chang Z, Cocke CL. Effects of molecular structure on ion disintegration patterns in ionization of O_2 and N_2 by short laser pulses. *Phys Rev Lett*. 2004;93:Article 113003.
39. Tong XM, Zhao ZX, Alnaser AS, Voss S, Cocke CL, Lin CD. Post ionization alignment of the fragmentation of molecules in an ultrashort intense laser field. *J Phys B Atomic Mol Phys*. 2005;38:333–341.
40. Li W, Jaroń-Becker AA, Hogle CW, Sharma V, Zhou X, Becker A, Kapteyn HC, Murnane MM. Visualizing electron rearrangement in space and time during the transition from a molecule to atoms. *Proc Natl Acad Sci USA*. 2010;107(47):20219–20222.
41. Pavičić D, Lee KF, Rayner DM, Corkum PB, Villeneuve DM. Direct measurement of the angular dependence of ionization for N_2, O_2 and CO_2 in intense laser fields. *Phys Rev Lett*. 2007;98:Article 243001.
42. Hu X, Jia C, Xu T, Wu Y, Wang J. Full quantum time-dependent simulations for the two-body breakups of H_2Ar^{2+} and N_2Ar^{2+}. *Phys Rev A*. 2022;106:Article 012814.
43. Murray R, Liu W-K, Ivanov MY. Partial Fourier-transform approach to tunnel ionization: Atomic systems. *Phys Rev A*. 2010;81:Article 023413.
44. Murray R, Spanner M, Patchkovskii S, Ivanov MY. Tunnel ionization of molecules and orbital imaging. *Phys Rev Lett*. 2011;106:Article 173001.
45. Xu H, He F, Kielpinski D, Sang R, Litvinyuk I. Experimental observation of the elusive double-peak structure in R-dependent strong-field ionization rate of H_2^+. *Sci Rep*. 2015;5:13527.
46. Liu H, Zhao SF, Li M, Deng Y, Wu C, Zhou XX, Gong Q, Liu Y. Molecular-frame photoelectron angular distributions of strong-field tunneling from inner orbitals. *Phys Rev A*. 2013;88:061401(R).
47. Sun S, Yang Y, Zhang J, Wu H, Chen Y, Zhang S, Jia T, Wang Z, Sun Z. Ejection of triatomic molecular ion H_3^+ from methyl chloride in an intense femtosecond laser field. *Chem Phys Lett*. 2013;581:16–20.